The Polarization-Dependent Relation Between Radar Backscatter from the Ocean Surface and Surface Wind Vector at Frequencies Between 1 and 18 GHz

C. M. H. Unal, P. Snoeij, and P. J. F. Swart

Abstract—**ESA's ERS-1 mission includes a *C*-band *VV* polarization wind scatterometer for which a wind-field-retrieval algorithm has been developed using a radar signature model CMOD1. A series of airborne scatterometer measurements were carried out in the framework of the EOPP (ESA's Earth Observation Preparatory Program) with the multifrequency airborne scatterometer DUTSCAT (TOSCANE-2 campaign 1987). The objective of this activity is to establish a multifrequency dual-polarization radar signature data base, and with it a multidimensional version of the current CMOD1 model. The main features of the data set are the following. The wind exponent γ of the upwind NRCS increases with frequency and incidence angle in the case of *HH* polarization. This trend is less noteworthy for *VV* polarization. The upwind/downwind ratio UD is mainly negative at 20° of incidence angle, always at *C*-, *X*-, and *Ku*1-bands. The difference ΔUD between *HH* and *VV* polarization is increasing with the incidence angle, except at *L*-band. The upwind/crosswind ratio UC increases with the incidence angle and varies very little with the polarization.**

Keywords—**Ocean surface, wind vector, radar backscatter, multifrequency, dual-polarization.**

NOMENCLATURE

U, C, D	Upwind, crosswind, downwind NRCS.
UC, UD	Upwind/crosswind, upwind/downwind ratios.
V	Horizontal wind-speed component in m/s at a height of 10 m above the sea surface in neutral stability conditions.
γ	V exponent for upwind NRCS.
σ°	NRCS.
θ	Incidence angle (degrees, with respect to vertical).
ϕ	Azimuth angle (zero for upwind).
Ω	Circle frequency in units 1/circle (it gives the number of sinusoidal oscillations per circle).

Manuscript received July 27, 1990; revised March 12, 1991.

The authors are with the Laboratory of Telecommunications and Remote Sensing, Delft University of Technology, P.O. Box 5031, 2600 GA Delft, The Netherlands.

IEEE Log Number 9100468.

I. INTRODUCTION

THE feasibility of microwave radar at medium incidence angles to estimate the instantaneous surface wind vectors depends upon well-established observations, partly backed by theory, that the radar sea echo responds rapidly to the local wind, and that the strength of the echo increases with wind speed and varies with the azimuth angle between the radar beam and wind direction. Microwave observations show echo extrema (maxima in the up- and downwind directions, and minima in the crosswind direction) and a smooth decrease of the echo with increasing incidence angle. The first full azimuth measurements come from airborne circle flight data [4] at *Ku*-band that were held in preparation of the SEASAT mission. The radar echo was seen to follow a near-perfect cosine variation of two cycles per azimuth circle. It was the start of establishing empirical models in order to translate the radar sea echo by easy inversion into estimates of the wind vector to use in satellite wind-retrieval algorithms. In spite of the above empirical evidence, the interaction mechanism between the ocean surface and microwave radiation is still subject of scientific debate. The practical implication of this uncertainty is that the limits of validity of the current models and the impacts of secondary influences (sea surface temperature, atmospheric stability, swell, surface films) are hard to predict. In view of this, a series of airborne scatterometer measurements were carried out in the framework of ESA's Earth Observation Preparatory Program (EOPP). This paper deals with the first results obtained from the analysis of these measurements. It summarizes the campaign, the data processing, and shows an example of output, constituting the data base. The empirical model CMOD1 is described and results of its multifrequency, dual-polarized version are given.

II. DATA ACQUISITION

The dual-polarization multifrequency TOSCANE-2 data set is acquired with the airborne scatterometer DUTSCAT (Delft University of Technology SCATterometer), which operates simultaneously at 6 frequencies

0196-2892/91/0700-0621$01.00

between 1 and 18 GHz. This coherent pulse radar uses as an antenna a single parabolic dish (diameter: 0.9 m) with a dual-polarized broadband feed. The across-track resolution is 20 m at an incidence angle of 45°, and the along-track resolution improves with increasing frequency from 200 to 10 m for 1 to 18 GHz at a flight altitude of 2000 ft and incidence angle 45°. For each frequency, 10 subsequent pulses are averaged to obtain the power values of 512 range samples (coherent integration). These sample values are accumulated 256 times (incoherent integration) and the results are recorded on tape once every 200 ms. A technical description of DUTSCAT can be found in [6].

TOSCANE-2 was performed over the Atlantic Ocean close to Bretagne (France) at the end of Autumn 1987 (from November 17 to December 4). Special emphasis was given to meteorological and surface data collection (surface wind, sea state, wave parameters) supplied by a research ship and a network of moored buoys. The input surface wind used is a 10-min-averaged wind speed (m/s) and direction (degree; geographic direction from which the wind is blowing) computed at the 10-m level above sea surface in neutral conditions using the boundary layer model [5]. For the azimuthal dependency of the NRCS (Normalized Radar Cross Section), circle flights were performed at three incidence angles, 20°, 30°, and 45°, using the two like-polarizations *HH* and *VV*. One circle flight has a diameter of 2 km and about 2-min duration. External calibration flights were carried out at the airfield Quimper in Bretagne using a set of corner reflectors. The strategy of measurements has been to switch from one like-polarization to the other one after 10 circles in order to have a meaningful comparison between *HH* and *VV* data. Accordingly, absolute NRCS data can be related to sea parameters in functions of frequency, polarization, incidence angle, and azimuth.

III. Data Processing

A. NRCS Calculation

The raw data (about 560 circles per frequency) consist of scatterometer data and flight data (angle of incidence, azimuth, altitude) as functions of time. Each recording or flight track consisting of 5 or 10 circles contains the data for a maximum of 6 frequencies, one polarization, and one incidence angle. Using the scatterometer data together with the flight data, the backscatter coefficient of the resolution cell located at the antenna beam axis can be calculated. Owing to the fact that DUTSCAT uses one antenna for all six frequencies, two types of data processing are employed. For the lower two frequencies (1.2 and 3.2 GHz), the antenna beamwidth is too large to neglect the possible variation of the scattering coefficient over the illuminated area. Using the range resolution a SLAR-like processing is performed. For the four remaining frequencies the antenna beamwidth is narrow enough that variations in the NRCS and range over the footprint of the antenna are small. Using a parabolic fit on the logarithmically converted range data, the received power for the antenna beam axis can be reconstructed.

B. Calibration

For distributed targets the echo power is a statistical quantity of which the average $\langle P \rangle$ is given by:

$$\langle P \rangle = C \cdot \sigma^{\circ} \cdot A \tag{1}$$

where A is the resolution cell, and C depends on the radar system parameters. The calibration requires system characterization to obtain the radar constant C. In DUTSCAT a delayed replica of the transmit pulse is used to monitor short-term system changes such as transmitted power and receiver gain fluctuations for the six frequencies separately. Antenna and illumination geometry are outside the internal calibration path. Therefore antenna tests and/or external calibration, where reference targets with known radar cross sections are measured, have to be performed. For airborne scatterometers external calibration is particularly difficult, because the influence of aircraft altitude and attitude variations through observation distance and antenna diagram are relatively large. Therefore this exercise is only feasible on days with calm weather. Arrays of square-based trihedral corner reflectors were used for TOSCANE-2. Their dimensions have been selected to insure a good S/N ratio based upon the radar resolution cell, size, and background contribution. An array rather than a single target is necessary, because it is difficult to control the aircraft track with sufficient precision to hit a single target with a narrow antenna beam in a controlled fashion. With multiple targets, several responses are used to reconstruct the measurement geometry at the time of calibration.

C. Average Circles

Processing output consists of six average circles per recording (one for each frequency). They contain the NRCS data for one like-polarization, one incidence angle, and one wind vector as a function of the azimuth angle, with the north as reference and with a resolution of 5°. Prior to the averaging step, a linear regression of NRCS versus incidence angle is performed per 5° azimuth interval in order to interpolate the NRCS values to predetermined nominal incidence angles. Typically, the range of variation of the incidence angle around the nominal one is 1°. It was required to stay within 2 km of a specified buoy that supplied a wind vector each 10 min with an accuracy of ± 1 m/s for the wind speed and $\pm 10°$ for the wind direction. The highest value of the wind speed V during the campaign was 15 m/s.

A filter is performed on the average circle: A low-pass filter (cut off $\Omega = 10.5$ circle^{-1}) and smoothing convolution algorithm (least-squares fitting over N local points) [3] which preserves the size, position, and shape of slowly varying features in comparison with the equivalent low-pass filter. From the smoothed average circle the upwind, downwind, and crosswind NRCS are extracted. A Fourier series development (cut off $\Omega = 10$ circle^{-1}) is then performed in order to calculate the power amplitudes C_i and phases ϕi in the respective harmonics. The azimuth angle ϕ and phases ϕi are related to the upwind direction.

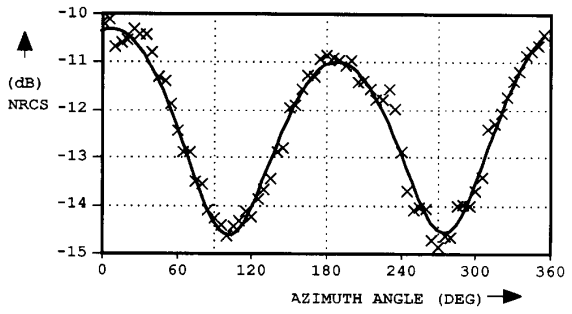

Fig. 1. Example of NRCS behavior versus azimuth angle.

Fig. 1 gives an example of an average circle. In this figure the NRCS (in dB) are plotted versus the azimuth (in degrees) with respect to the north for the frequency of 3.2 GHz. The average circle is fitted by the following function:

$$C_0 \cdot (1 + C_1 \cdot \cos(\phi - \phi_1) + C_2 \cdot \cos(2\phi - \phi_2)). \tag{2}$$

It corresponds to the three first terms of the Fourier series development. For all the observations this is a good description, since on average the percentage of power in the first two harmonics appears to be in the range of 89–96%, 89% for the *L*-band and 96% for the *C*-band.

In summary, the processing output per recording consists of:

- Average circle versus measurement conditions (wind, polarization, etc.)
- Mean level of the NRCS
- Position and NRCS of extrema (up-, down-, cross-wind)
- Extrema ratios (upwind/downwind, etc.)
- Complex spectrum (cut off at $\Omega = 10$ circle^{-1})
- Quality statistics: Number of circles, percentage of outliers and missing points, standard deviation of the NRCS per azimuth interval of 5°, power combined in harmonics $\Omega = 1$ circle^{-1} and $\Omega = 2$ circle^{-1}.

IV. Model CMOD1

A. Formulation

An international experimental ESA campaign in 1984 has led to the formulation of an empirical model CMOD1 at *C*-band and *VV* polarization. This campaign is known as the *C*-band campaign [1], [2]. The CMOD1 model relates the NRCS to the surface wind vector, the incidence and azimuth angles [3]. This model forms the basis of the wind retrieval algorithm of ERS-1. The following describes the CMOD1 model.

The model assumes that the NRCS can be factorized into an absolute factor, which is here the upwind NRCS and a relative azimuthal factor:

$$\sigma^\circ = U \cdot (1 + B_1 \cdot \cos\phi + B_2 \cdot \cos 2\phi)/(1 + B_1 + B_2) \tag{3}$$

$$U = B_0 \cdot V^\gamma. \tag{4}$$

The parameters B_0 and γ are slowly varying functions of θ, and the parameters B_1 and B_2 are slowly varying functions of both θ and V. The denominator in (3) is introduced to make the relative azimuthal factor equal to 1 when ϕ is 0°. The use of the ratios UC and UD instead of B_1 and B_2 gave better fitting results for the ESA *C*-band campaign [3]. Therefore the same procedure is used for TOSCANE-2 data. Expansions are required for log U (log to get a linear fitting), UC, and UD in terms of θ and V. A possible V dependence for UC and UD has been assumed to be linear. These V-dependent terms have coefficients dependent on θ. The θ-dependent terms are expanded as 2nd-order Legendre polynomials as follows:

$$\log U = \sum_{i=0}^{2} l_i \cdot P_i(x) + \sum_{i=0}^{2} m_i \cdot P_i(x) \cdot \log V \tag{5}$$

$$UC = \sum_{i=0}^{2} n_i \cdot P_i(x) + \sum_{i=0}^{2} p_i \cdot P_i(x) \cdot V \tag{6}$$

$$x = (2\theta - \theta_2 - \theta_1)/(\theta_2 - \theta_1) \tag{7}$$

$$B_1 = 2 - 4 \cdot (1 + \mathrm{UC}/\mathrm{UD})/(2 + \mathrm{UC}/\mathrm{UD} + \mathrm{UC}) \tag{8}$$

$$B_2 = 1 - 4/(2 + \mathrm{UC}/\mathrm{UD} + \mathrm{UC}). \tag{9}$$

The l_i, m_i, n_i, and p_i are expansion coefficients determined by least-squares fitting of the data. The Legendre expansion is in terms of the normalized quantity x, where x follows in the case of TOSCANE-2 from the range $\theta_1 = 20°$ to $\theta_2 = 45°$. The expansion for UD is of the same form of UC.

B. Results and Conclusions

For ease of comparison, the conclusions of the *C*-band campaign of which the data base was used to fit CMOD1 are summarized in this paragraph [3]. CMOD1 gave an accuracy in wind speed of ±2 m/s for the *C*-band data base. For the upwind NRCS, points of interest were the wind speed exponent γ, which increased with θ and leveled off at about 1.48 at 60°, but was below unity for $\theta < 30°$. The values of γ were somewhat lower than those found for the *Ku*-band scatterometer of SEASAT. The UC ratio with $\theta > 20°$ increased with both θ and V. The UD ratio showed similar trends to the UC ratio. The less-than-unity values below 20° were noteworthy and a definite speed dependence appeared above about 40°. The UC and UD ratios were similar in magnitude for *C*- and *Ku*-bands. It was noticed that the values for the NRCS were 2-dB higher than in the *Ku*-band.

V. Results of the TOSCANE-2 Multidimensional Version of CMOD1

In this chapter we will limit ourselves to a discussion of the main features of our data set. For more detailed quantitative information of the CMOD1 multifrequency and two-polarization parameters, the reader is refered to [7].

TABLE I
WIND EXPONENT γ FOR THE UPWIND NRCS

(a) *HH*-polarization: Frequency (GHz)					
$\theta(°)$	1.2	3.2	5.3	13.7	17.25
20	0.48	0.67	0.76	0.86	1.06
30	0.92	1.29	1.32	1.95	1.66
45	0.76	1.38	1.40	1.43	—
(b) *VV*-polarization: Frequency (GHz)					
$\theta(°)$	1.2	3.2	5.3	13.7	17.25
20	0.67	0.84	0.70	1.10	1.11
30	0.53	1.04	1.41	1.81	1.56
45	0.47	1.04	1.65	1.15	0.84

a) *HH* polarization. b) *VV* polarization.

A. Wind Exponent γ

The results of the fit giving the wind-speed exponent γ for the upwind NRCS are presented in the Table I. γ increases with the frequency for the polarization *HH*. This trend is not always found in case of the polarization *VV*. The value of $\gamma(VV)$ at 45° is an example of *C*-band having a higher wind-speed sensitivity than *Ku*-band. There is a trend for γ to increase with the incidence angle at *HH*-polarization, which is less pronounced at *VV*-polarization (the only increase on the total range of incidence angles is at *C*-band). The sensitivity for the wind speed is higher for *HH* than *VV* at 30° and 45° (not for *C*-band).

B. Average NRCS

Fig. 2(a)-(c) gives the behavior of the average NRCS in dB versus the frequency for the two like-polarizations at a wind speed of 10 m/s. The 5 marker points represent, respectively, *L*-, *S*-, *C*-, *Ku*1-, and *Ku*2-bands. No absolute value for *X*-band is given in consequence of a problem of calibration. The dashed curve represents *VV*-polarization. The shape of the curves appears to be independent of the wind speed from 6 to 14 m/s.

Table II gives the mean NRCS difference between *VV*- and *HH*-polarization, $\Delta\sigma°$, in function of the incidence angle, frequency, and windspeed. Because of erroneous data at *Ku*2-band for the following conditions, *HH*-polarization and 45° of incidence angle, this information is absent in Table II. A distinction in behavior appears between 20° of incidence angle and 30°, 45°. In the typically Bragg-scattering region (30°, 45°), the trend is a decrease of $\Delta\sigma°$ with increasing wind speed for all frequencies except *C*-band, where the opposite behavior is noticed. This difference of behavior of *C*-band compared to the other frequencies, which is also present at 20°, has not yet been explained. Measurements at *X*-band in the Delft Hydraulics wind/wave tank [8], resulting in $\Delta\sigma°$ versus wind speed, show a difference between the two like-polarizations at 45° of incidence angle which increases with the wind speed until the appearance of breaking waves. As soon as this degree of roughness is reached, $\Delta\sigma°$ will decrease with increasing wind speed. In open sea the waves are not purely generated by the measured wind,

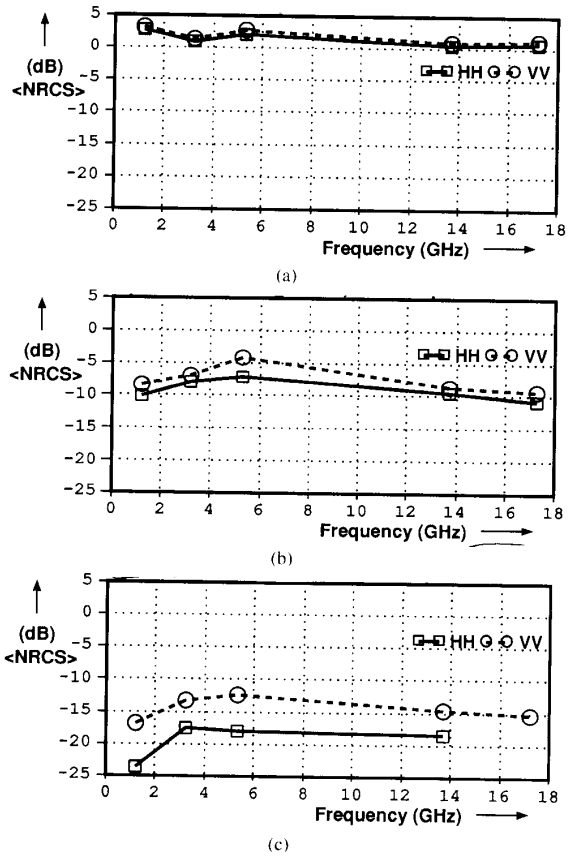

Fig. 2. Average NRCS versus frequency for the two like-polarizations. (a) Incidence angle 20°, windspeed 10 m/s. (b) Incidence angle 30°, windspeed 10 m/s. (c) Incidence angle 45°, windspeed 10 m/s.

and it can happen to have a rough sea while a low wind is blowing. It can be an interpretation of the fact that only the second trend, after breaking, is visible from the TOSCANE-2 data set.

The expected behavior of $\Delta\sigma°$ should increase for increasing incidence angle is verified: At 20° $\Delta\sigma°$ is typically half a dB or less, at 30° (excluding *C*-band with a $\Delta\sigma°$ of 2.5 dB) 1-dB average, and at 45° it is from 4 to 5 dB. The variation of $\Delta\sigma°$ with the frequency increases with the incidence angle and at low wind speeds. This parameter $\Delta(\Delta\sigma°)$ is relatively stable as function of frequency at 20° and 30°, excluding *C*-band.

C. Upwind/Downwind

Figs. 3(a)-(c) gives the behavior of UD in dB versus the frequency for the two like-polarizations at a wind speed of 10 m/s. Summarizing all wind speed cases, we find that UD increases with the incidence angle at *HH*-polarization with an exception for *L*-band, whereas this trend is slight at *VV*-polarization where a maximum in UD is mainly found for 30° at *S*-, *X*-, *Ku*1-, and *Ku*2-bands. For wind speeds of 10 m/s and higher, the trend of the increase of UD with the incidence angle is present at *VV*-polarization at *L*-, *C*-, *X*-, *Ku*1-, and *Ku*2-

TABLE II
MEAN NRCS DIFFERENCE BETWEEN *VV*- AND *HH*-POLARIZATION IN dB FOR 20, 30, AND 45° ANGLE OF INCIDENCE

20° Freq. (GHz)	Wind speed (m/s)						
	2	4	6	8	10	12	14
1.2	−0.94	−0.38	−0.05	0.18	0.35	0.50	0.63
3.2	−0.24	0.06	0.18	0.26	0.32	0.36	0.39
5.3	1.05	0.79	0.65	0.56	0.51	0.49	0.49
13.7	−1.33	−0.58	−0.14	0.19	0.45	0.67	0.86
17.25	−0.21	−0.01	0.14	0.27	0.38	0.49	0.59
30° Freq. (GHz)	Wind speed (m/s)						
	2	4	6	8	10	12	14
1.2	4.18	3.06	2.40	1.94	1.59	1.29	1.03
3.2	2.43	1.79	1.42	1.18	0.98	0.82	0.68
5.3	2.07	2.37	2.57	2.70	2.80	2.88	2.95
13.7	1.97	1.55	1.29	1.12	0.99	0.87	0.76
17.25	1.96	1.72	1.59	1.51	1.45	1.39	1.36
45° Freq. (GHz)	Wind speed (m/s)						
	2	4	6	8	10	12	14
1.2	9.44	8.35	7.67	7.15	6.73	6.38	6.07
3.2	6.88	5.76	5.08	4.60	4.22	3.91	3.66
5.3	4.78	5.25	5.47	5.59	5.66	5.71	5.75
13.7	5.70	4.86	4.37	4.02	3.76	3.56	3.39
17.25	—	—	—	—	—	—	—

a) 20°. b) 30°. c) 45°.

bands. In correspondance with the *C*-band campaign results, an increase of UD with the incidence angle is found for *C*-band and *VV*-polarization. It is important to note that UD is mainly negative at 20°, and that this is always the case for *C*-, *X*-, and *Ku*1-bands.

The variation of UD with the frequency decreases with increasing wind speed up until a minimum, located mainly at 10 m/s (in two cases at 12 m/s) to increase afterwards with the wind speed. The average variation of UD with the frequency is half a dB at 20° and 45° of incidence angle. It is higher at 30° with a value of 1 dB at *VV*-polarization and 1.8 dB at *HH*-polarization.

The upwind/downwind difference between *HH*- and *VV*-polarization ΔUD in dB is increasing with the incidence angle for all the frequencies except *L*-band. In the Bragg-scattering region of 30° and 45°, ΔUD is decreasing with increasing wind speed but is always positive. However, for the 30° incidence-angle case, there are two exceptions: *Ku*2-band, where ΔUD is independent of the wind speed, and *L*-band, where ΔUD is negative. In summary, all curves of ΔUD versus wind speed are monotonically decreasing for all the frequencies at 30° and 45° except for the *Ku*2-band 30° case.

D. Upwind/Crosswind

Figs. 4(a)–(c) reflects the behavior of the upwind/crosswind ratio in dB versus the frequency for the two like-polarizations at a windspeed of 10 m/s. UC is increasing with the incidence angle and generally also with the wind speed. This conclusion of the *C*-band campaign can be extended to *L*-, *S*-, *X*-, and *Ku*2-bands. A slow decrease of UC while increasing windspeed has been noticed but not explained at *Ku*1-band at 30° (*HH*-polarization) and 30°–45° at *VV* polarization. At low windspeeds (2–4 m/s), it barely happens that UC does not increase with the incidence angle.

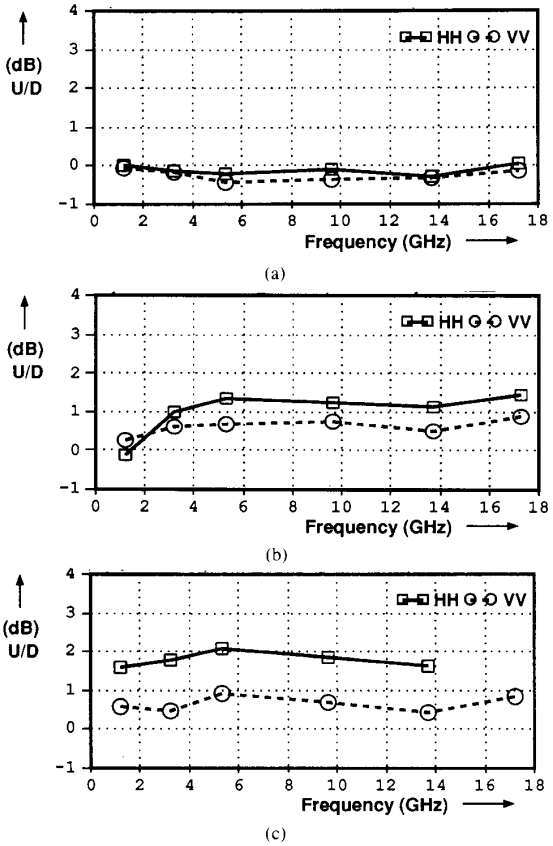

Fig. 3. Upwind/downwind ratio versus frequency. (a) Incidence angle 20°, windspeed 10 m/s. (b) Incidence angle 30°, windspeed 10 m/s. (c) Incidence angle 45°, windspeed 10 m/s.

A minimum value of UC is found at *L*-band. The maximum values of the ratios UC and UD are mainly found at *Ku*-band (*Ku*2-band for UD) and *C*-band (*C*-band at 45° of incidence angle and for 12 m/s and higher wind speeds at 30°). The variation of UC with the frequency has an average value of maximally 2 dB for the 20° and 45°-*HH* cases, and a little bit higher in the other cases (≤3 dB for the 30° and 45°-*VV* cases).

The difference ΔUC between the two like-polarizations is found to be rather small, reaching until 1 dB for low wind speeds and 45° of incidence angle.

VI. CONCLUSIONS

The objectives of the TOSCANE-2 campaign are satisfied. A multifrequency dual-polarized radar signature of the ocean database is obtained and a multidimensional version of the CMOD1 model has been established. Comparisons with earlier obtained *C*-band data and also

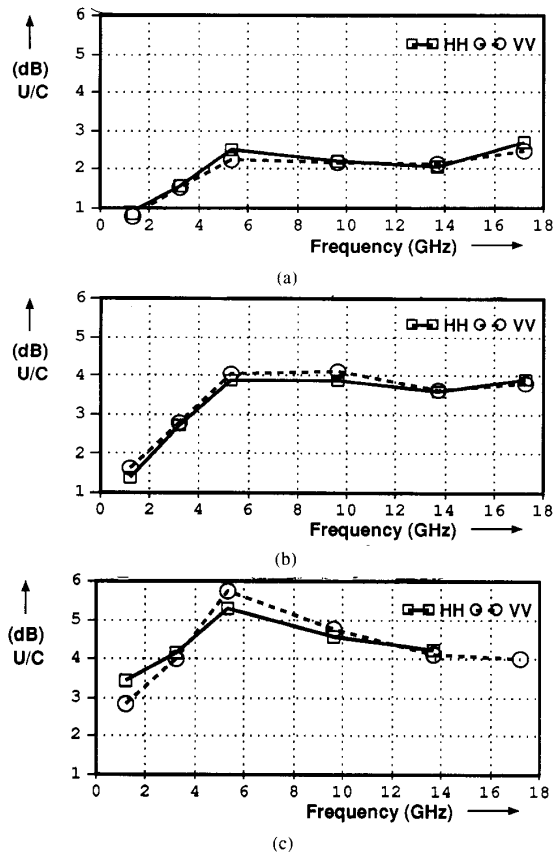

Fig. 4. Upwind/crosswind ratio versus frequency. (a) Incidence angle 20°, windspeed 10 m/s. (b) Incidence angle 30°, windspeed 10 m/s. (c) Incidence angle 45°, windspeed 10 m/s.

Ku-band (SEASAT) data indicate that a valuable data set is acquired. A first analysis of the fitting model results has been performed. Further analyses are and will be carried out from this dataset in order to improve the use of satellite remotely sensed data of the sea. The obtained model can be used in theoretical studies of the sea-scattering mechanisms. A summary of the main conclusions of our first analysis of the TOSCANE-2 data set is given below.

The wind exponent γ of the upwind NRCS increases with frequency and incidence angle in the case of *HH*-polarization. This trend is less noteworthy for *VV*-polarization. In the typical Bragg-scattering region (30°, 45°), the sensitivity of NRCS on wind speed is higher for *HH* than *VV*, except at *C*-band.

The upwind/downwind ratio UD is mainly negative at 20° of incidence angle, always at *C*-, *X*-, and *Ku*1-bands. The difference ΔUD between *HH* and *VV* polarization is increasing with the incidence angle except at *L*-band. ΔUD versus wind speed is monotonically decreasing for all the frequencies at 30° and 45°, except in the *Ku*2-band 30° case. The upwind/crosswind ratio UC increases with the incidence angle and varies very little with the polarization. The maximum values of the ratios UC and UD are mainly found at *Ku*-band (*Ku*2-band for UD) and *C*-band (*C*-band at 45° of incidence angle and for a 12 m/s and higher wind speed at 30°).

References

[1] E. P. W. Attema, "An experimental campaign for the determination of radar signature of the ocean at *C*-band," in *Proc. 3rd Int. Coll. Spectral Signatures of Objects in Remote Sensing* (Les Arcs, France), 16–20 Dec. 1985, pp. 3–10.

[2] G. P. De Loor, "Analysis of the ESA windscatterometer campaign data," in *Proc. 3rd Int. Coll. Spectral Signatures of Objects in Remote Sensing* (Les Arcs, France), 16–20 Dec. 1985, pp. 73–76.

[3] A. E. Long, "Towards a *C*-band radar sea echo model for the ERS-1 Scatterometer," in *Proc. 3rd Int. Coll. Spectral Signatures of Objects in Remote Sensing* (Les Arcs, France), 16–20 Dec. 1985, pp. 29–34.

[4] R. K. Moore and A. K. Fung, "Radar determination of winds at sea," *Proc. IEEE*, vol. 67, pp. 1504–1521, Nov. 1979.

[5] P. Queffeulou *et al.*, "TOSCANE-2 campaign report IFREMER contribution," ESA ESTEC, Noordwijk, The Netherlands, Contract 7138/87/NL/BI, 1988.

[6] P. Snoeij and P. J. F. Swart, "The DUT airborne scatterometer," *Int. J. Remote Sensing*, vol. 8, no. 11, pp. 1709–1716, 1987.

[7] C. M. H. Unal and P. Snoeij, "TOSCANE-2 Progress Report 2," ESA, Contract 8722/89/F/FL(SC), 1990.

[8] D. Van Halsema *et al.*, "Experiment and first results," in *Progress Report on the VIERS-1 Project, Part 1: The Delft Wind/Wave Experiment*, Netherlands Remote Sensing Board, Delft, The Netherlands, Rep. BCRS-89-24.

C. M. H. Unal received the D.E.A. degree in the physics for remote sensing from the University of Paris in 1987.

She joined the Delft University of Technology, Delft, The Netherlands, in 1988, where she works as a Research Scientist. She has been working on microwave remote sensing, and her current research field is in radar polarimetry.

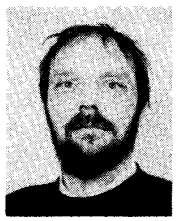

Paul Snoeij was born in Rotterdam, The Netherlands, on May 5, 1953. He received the M.Sc. degree in electrical engineering in 1982 from the Delft University of Technology, Delft, The Netherlands.

He joined the Delft University of Technology in 1978. Since 1981 he has been working on microwave remote sensing, with special emphasis on the design of SLAR, SAR, and scatterometer systems and on object-sensor interaction studies for the design of optimum sensors.

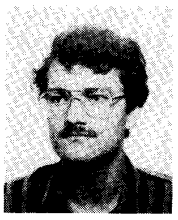

P. J. F. Swart was born in Amsterdam, The Netherlands, in 1960. He received the M.Sc. degree from the Delft University of Technology, Delft, The Netherlands, in 1985.

Since then he has been active in several areas of microwave remote sensing, including data processing, modeling, and in-door RCS measurements at what was formerly called the Microwave Laboratory of TU-Delft.